Surface flatness and distortion inspection of precast concrete elements using laser scanning technology

Qian Wang[1,2], Min-Koo Kim[3], Hoon Sohn[2] and Jack C.P. Cheng[*1]

[1]*Department of Civil and Environmental Engineering, The Hong Kong University of Science and Technology, Clear Water Bay, Kowloon, Hong Kong*
[2]*Department of Civil and Environmental Engineering, Korea Advanced Institute of Science and Technology, 291 Daehak-ro, Yuseong-gu, Daejeon 34141, Republic of Korea*
[3]*Department of Engineering, University of Cambridge, Cambridge, England, United Kingdom*

Abstract. Precast concrete elements are widely used in the construction of buildings and civil infrastructures as they provide higher construction quality and requires less construction time. However, any abnormalities in precast concrete surfaces such as non-flatness or distortion, can influence the erection of the elements as well as the functional performance of the connections between elements. Thus, it is important to undertake surface flatness and distortion inspection (SFDI) on precast concrete elements before their delivery to the construction sites. The traditional methods of SFDI which are conducted manually or by contact-type devices are, however, time-consuming, labor-intensive and error-prone. To tackle these problems, this study proposes techniques for SFDI of precast concrete elements using laser scanning technology. The proposed techniques estimate the F_F number to evaluate the surface flatness, and estimate three different measurements, warping, bowing, and differential elevation between adjacent elements, to evaluate the surface distortion. The proposed techniques were validated by experiments on four small scale test specimens manufactured by a 3D printer. The measured surface flatness and distortion from the laser scanned data were compared to the actual ones, which were obtained from the designed surface geometries of the specimens. The validation experiments show that the proposed techniques can evaluate the surface flatness and distortion effectively and accurately. Furthermore, scanning experiments on two actual precast concrete bridge deck panels were conducted and the proposed techniques were successfully applied to the scanned data of the panels.

Keywords: flatness inspection; distortion inspection; precast concrete elements; laser scanning; bridge deck panels

1. Introduction

Precast concrete elements are widely used for the construction of buildings and civil infrastructures as precast concrete allows higher construction quality, shorter construction time, and less environmental impact compared to cast-in-place concrete (Glass 2000, Alhassan 2011, Yee and Eng 2001). However, it is important to ensure the surface quality of precast concrete

---

∗Corresponding author, Assistant Professor, E-mail: cejcheng@ust.hk

elements before their delivery to the construction sites. It was reported that any surface abnormalities of precast concrete elements such as non-flatness or distortion can influence (1) the visual features of the elements, (2) the ease of erection of the elements, and (3) the functional performance of the connections between elements (Alhassan 2011). Furthermore, the poor quality of connections between elements can result in serious deterioration problems in the long term, as reported in several precast concrete cases (Wacker *et al.* 2005).

Flatness and distortion are two important aspects of precast concrete surface quality. Surface flatness measures the deviation in elevation of a surface over short distances, while surface distortion measures the overall out-of-plane curvature of a planar surface (PCI 2000, BSI 2009). Surface flatness is a characteristic of the local surface smoothness, while surface distortion is a characteristic of the entire surface shape (PCI 2000). Fig. 1 shows the cross section views of a typical non-flat surface and a distorted surface.

Surface flatness directly relates to the deviation in elevation of the surface. Assuming a roughly horizontal surface, surface distortion can also be obtained from the elevation of the surface. Thus, inspection of both surface flatness and distortion requires elevation measurements throughout the surface. In practice, a few sample points are usually determined on the surface and the elevations of the sample points are collected to measure the surface flatness and distortion. In general, two types of apparatuses are used for measuring the elevations of sample points (ASTM 2008, Ballast 2007). The first type measures the elevation of a point, and includes leveled straightedges, optical levels, laser levels, floor profilometers, etc. The second type measures the elevation difference between a pair of points, and includes inclinometers, longitudinal differential floor profilometers, etc. In addition, measuring tapes are sometimes necessary as an ancillary equipment. The above-mentioned traditional inspection methods are conducted manually or by contact-type devices, and have mainly two limitations. Firstly, it is time-consuming and labor-intensive, especially when the surface has a large area and contains a large number of sample points, as the elevations of the sample points need to be measured and recorded one by one. Secondly, it is error-prone as it involves a lot of tedious manual work (Phares *et al.* 2004). Hence, it is necessary to provide solutions that can conduct surface flatness and distortion inspection (SFDI) more efficiently and accurately.

Recently, 3D laser scanners have become popular as a novel type of non-contact range sensors. A laser scanner measures the distance to a target object by emitting laser beams and detecting the reflected signals from the target object (Amann *et al.* 2001).
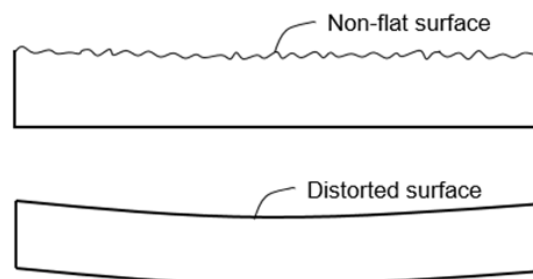

Fig. 1 Illustrative examples of surface flatness and distortion

Compared to traditional range sensors, 3D laser scanners have the advantages of high measurement accuracy (e.g., ±2 mm at a scanning distance of 20 m) and high measurement speed (e.g., 976,000 points per second) (FARO, 2015). As a result of these benefits, 3D laser scanners have been used in various civil engineering applications including the reconstruction of 3D as-built models (Bosché *et al.* 2015, Xiong *et al.* 2013), construction progress tracking (El-Omari and Moselhi 2008, Turkan *et al.* 2012) and construction quality inspection (Kim *et al.* 2014, Bosché 2010, Tang *et al.* 2010, Bosché and Guenet 2014). On the other hand, vision-based and GPS-based approaches are also widely used for the structure health monitoring of civil structures, as reported in several studies (Teza *et al.* 2009, Bai *et al.* 2015, Yeum and Dyke 2015, Yi *et al.* 2013a, b). Although these approaches are more economical, they are not as accurate as laser scanning. Therefore, this study focuses on laser scanning based approaches.

Some studies have been reported on surface flatness inspection using laser scanned data. Bosché and Guenet (2014) applied two commonly used flatness measurement methods, namely the Straightedge method and the F-Numbers method, to the laser scanned data of two concrete slabs. The experimental results showed that laser scanners can provide data with sufficient accuracy to perform surface flatness measurement. However, this previous study did not verify the F-Numbers results obtained from the laser scanned data by comparing them to the true values. Bosché and Biotteau (2015) recently applied the Continuous Wavelet Transform (CWT) method to the laser scanned data of a surface. Based on CWT, frequency analysis is conducted on the surface flatness. The CWT method provides results with higher resolution in the frequency domain compared to the Waviness Index method, which is an existing method that only considers five different frequencies. Nonetheless, the correlations between the proposed method and other standard flatness measurement methods have not yet been established, which limits the adoption of the proposed method in practice.

On the other hand, no study has measured surface distortion of precast concrete elements using laser scanned data. However, several studies (Park *et al.* 2007, Monserrat and Crosetto 2008) have measured the deformations of concrete surfaces, which refer to the changes of surface shapes at different time. Compared to surface deformation, measuring of surface distortion is different. For surface deformation, there are usually at least two sets of laser scanned data, one reference data and one target data, and the deformation is measured by comparing the two sets of data. Similarly, for surface distortion, it should be measured by comparing the current surface (target data) to the true plane (reference data), which is the true position of the surface when there is no distortion. However, once any distortion occurs, the true plane of a surface cannot be found any more. Hence, it is impossible to directly compare the current surface to the true plane. Instead, specific measurements are needed to indirectly evaluate the surface distortion of precast concrete elements. Some standard measurements that evaluate surface distortion have been defined and suggested by relevant industry associations, including the Precast/Prestressed Concrete Institute (PCI), the American Concrete Institute (ACI) and the American Society for Testing and Materials (ASTM), but no study has applied laser scanned data to estimate these measurements.

To tackle the limitations in the current research, this study proposes and validates techniques that use laser scanning technology to conduct SFDI of precast concrete elements. Surface flatness is measured by the F_F number in the F-Numbers method, while surface distortion is measured by three different measurements, warping, bowing and differential elevation between adjacent elements. The uniqueness of this study includes (1) the development of techniques to conduct SFDI using laser scanning technology, (2) the validation of the developed techniques by comparing the measured flatness and distortion from the laser scanned data with the actual ones, which is realized by using

3D printed test specimens, and (3) the adoption of three measurements to evaluate surface distortion in different aspects, considering both the individual precast concrete elements and complete precast concrete systems. This paper is organized as follows. Section 2 describes the measurements of surface flatness and distortion used in this study. Then, the proposed SFDI techniques are described in Section 3. Subsequently, Section 4 validates the proposed techniques with scanning experiments on small scale test specimens. In Section 5, the proposed techniques are applied to the laser scanned data of two actual precast concrete bridge deck panels. Lastly, Section 6 concludes this study and suggests future work.

2. Measurements of surface flatness and distortion

To quantitatively evaluate surface flatness and distortion, four different measurements of surface flatness and distortion are determined. All the measurements are standardized and suggested by PCI, ACI or ASTM. The details including the definition, the measurement method, and the tolerance value or reference value of each measurement are described as follows.

2.1 Measurement of surface flatness

In order to measure the flatness of concrete floor surfaces, ACI 117 (ACI 2006) specifies two standard methods, the 10-foot Straightedge method and the F-Numbers method. The 10-foot Straightedge method is performed by (1) placing a freestanding 10 feet (3 m) straightedge anywhere on the floor surface and allowing it to rest upon two supporting points, and (2) measuring the gap between the straightedge and the floor surface at any point between the two supporting points. Subsequently, the measured gap is used to classify the surface flatness into different classes. Although the Straightedge method has been used for more than 50 years, it has several deficiencies (Ballast 2007, ACI 2006). The major deficiency is the absence of standard protocol to measure deviations in lengths less than 10 feet (3 m). Consequently, elevation deviations over shorter distances can be neglected and surfaces with different levels of flatness may have the same measurement result using a 10-foot Straightedge. In addition, the 10-foot Straightedge method does not specify the sampling method on a surface, resulting in difficulties of measuring large surface areas and random sampling of surfaces. As the other option of surface flatness measurement, the F-Numbers method is relatively new compared to the Straightedge method. According to ASTM E 1155 (ASTM 2008), the F-Numbers method contains two ratings, the Floor Flatness (F_F) number and the Floor Levelness (F_L) number. The F_F number measures the degree to which a surface approximates a plane whereas the F_L number measures the degree to which a surface is horizontal. Note that the F_L number is applicable only to floors which are placed horizontally. Since the F_L number does not relate to surface flatness, only the F_F number is discussed in the following. The F_F number of a surface is obtained by the following three steps, (1) obtaining the elevations of a few sample points at intervals of 300 mm, (2) computing the curvatures between all the sample points at intervals of 600 mm, and (3) computing the F_F number as a statistical measure of these curvatures. The F_F number is advantageous over the Straightedge method in three aspects (ACI 2006). Firstly, the interval between two sample points (300 mm) is much smaller than that of the Straightedge method (3 m), thereby reflecting elevation deviations over much shorter distances. Secondly, since the sample points are distributed throughout the whole surface, the F_F number can reflect the flatness of the whole surface rather than a local area.

Thirdly, the F_F number specifies the method of placing sample points on surfaces, which facilitates random sampling of surfaces. For these advantages over the other method, the F_F number is selected as the measurement of surface flatness in this study.

The detailed procedure of determining the F_F number of a test surface according to ASTM E 1155 (ASTM 2008) is illustrated as follows.

(1) Place the sample measurement lines on the test surface, as shown in Fig. 2. The orientations of the lines should all be $45°$ to the longest boundary of the surface, or, parallel to or perpendicular to the longest boundary. Equal number of lines should be placed in two perpendicular directions. The lengths of lines should not be smaller than 3,300 mm and the distance between two parallel lines should not be smaller than 1,200 mm. (2) Subdivide each sample measurement line into 300-mm long intervals, and the points marking the ends of these intervals are named sample reading points.(3) Measure the elevations of the sample reading points (or the elevation difference between all adjacent sample reading points). For sample measurement line j, denote all sample reading points along it as $P_0, P_1, P_2, \ldots P_{n-1}, P_n$ and their elevations in millimeters as $h_0, h_1, h_2, \ldots h_{n-1}, h_n$ correspondingly. (4) Calculate the F_F number of each sample measurement line. For sample measurement line j, calculate the profile curvatures, q_i, between all sample reading points separated by 600 mm as $h_i - 2h_{i-1} + h_{i-2}$, where $i = 2, 3, 4 \ldots n$. Subsequently, the F_F number of sample measurement line j, denoted as F_j, is estimated by

$$F_j = \frac{115.8454}{3S_{q_i} + \left| \overline{q_i} \right|} \tag{1}$$

where S_{q_i} and $|\overline{q_i}|$ denote the standard deviation and the absolute value of the mean of all $(n-1)$ q_i values, respectively. (5) Calculate the F_F number of the test surface by combining all of the F_F numbers of individual sample measurement lines within the test surface. The details of the combining procedures can be found in ASTM E 1155 (ASTM 2008).

Based on the obtained F_F number, a surface can be classified into different classes. ACI (2006) provides the minimum F_F number required for four classes of floor surfaces, as shown in Table 1. Note that a larger F_F number indicates a flatter surface.
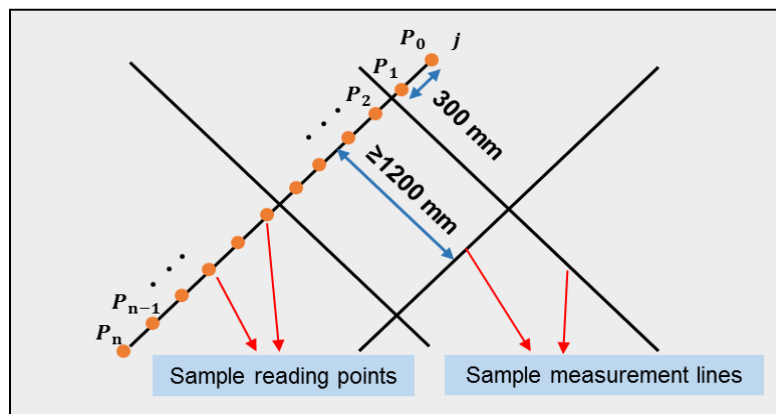

Fig. 2 Determination of the FF number of a test surface

Table 1 Floor surface classification based on the F_F number

Floor surface classification	Minimum F_F number
Bullfloated	15
Straightedged	20
Flat	30
Very flat	50

2.2 Measurements of surface distortion

According to PCI (2000), warping and bowing describe two different kinds of surface distortion and thereby can be used to evaluate the surface distortion of individual precast concrete elements in two different aspects. In addition, the surface distortion of individual precast concrete elements can result in the mismatching of two adjacent elements. Hence, the differential elevation between adjacent elements is selected as another measurement of surface distortion, as it evaluates the influence of the surface distortion on complete precast concrete systems. Therefore, a total of three measurements including warping, bowing, and differential elevation between adjacent elements are selected as the measurements of surface distortion in this study.

2.2.1 Warping

Warping refers to the twisting of a precast concrete element, resulting in overall out-of-plane curvature of surfaces characterized by non-parallel edges, according to PCI (2000). Warping of a surface is measured as the deviation of a corner from the plane containing the other three corners, as illustrated in Fig. 3. Hence, warping of a surface can be measured at four corners. If the corner is higher than the plane, the warping has a positive value; on the other hand, if the corner is lower than the plane, the warping has a negative value. The tolerance value of warping is usually proportional to the distance from the corner to its nearest adjacent corner, but the proportion varies for different types of precast concrete elements. For example, the tolerance value of warping for wall panels is 1/16 inch per foot (1.5 mm per 300 mm) of the distance to its nearest adjacent corner.
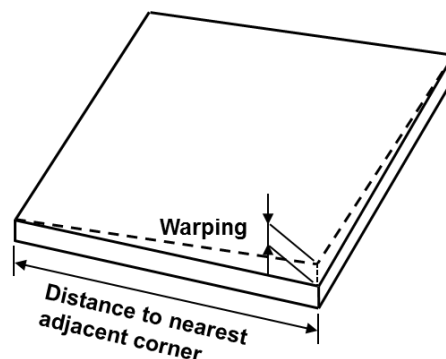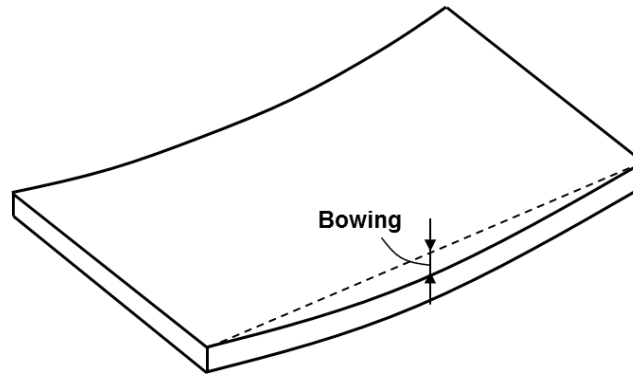

Fig. 3 Measurement of warping of a surface

Fig. 4 Measurement of bowing of a surface

2.2.2 Bowing

Bowing refers to an overall out-of-planeness condition which differs from warping in that, while two edges of the panel may fall in the same plane, the portion of the surface between the two edges is out-of-plane (PCI 2000). As shown in Fig. 4, although the two short edges are parallel and lie in the same plane, the surface between them is out of the plane. Bowing is measured as the deviation of an edge from the line containing the two endpoints of the edge. Hence, bowing of a surface can be measured along the four edges of the surface. If the edge is higher than the line, the bowing has a positive value; on the other hand, if the edge is lower than the line, the bowing has a negative value. The tolerance value of bowing is usually proportional to the length of the edge but has a maximum value. For example, the tolerance value of bowing for wall panels is length/360, but it cannot exceed 1 inch (25 mm).

2.2.3 Differential elevation between adjacent elements

Complete precast concrete systems are assembled by a series of individual precast concrete elements. The connections between adjacent elements play an important role in the performance of complete precast concrete systems. Hence, it is important to assess the quality of the connections between adjacent elements. Assuming that two elements are supposed to be placed adjacently on the same supporting plane (e.g., plane of girders for bridge deck panels) and to be connected at the same elevation. In this case, the differential elevation between adjacent elements is measured to evaluate the connection between the two elements.

The differential elevation is measured by two steps. Firstly, determine the erected orientations of elements on the supporting plane. If an element is well manufactured, all the four corners can be placed on the supporting plane. However, if any distortion exists, the four corners may not be in the same plane. Hence, the erected orientation should be determined based on the surface distortion of each element. Secondly, measure the elevation difference between the top surfaces of the two adjacent elements along the connected edge. Fig. 5 shows an example to illustrate the measurement of differential elevation, where two adjacent bridge deck panels are supposed to be placed on the same girders. It is assumed that panel A and panel B both have bowing along the longer edges but no bowing along the shorter edges. Therefore, the four corners of each panel are still in the same plane and can be placed on the girders. Then, the elevation difference between two panels is measured along the connected edge.
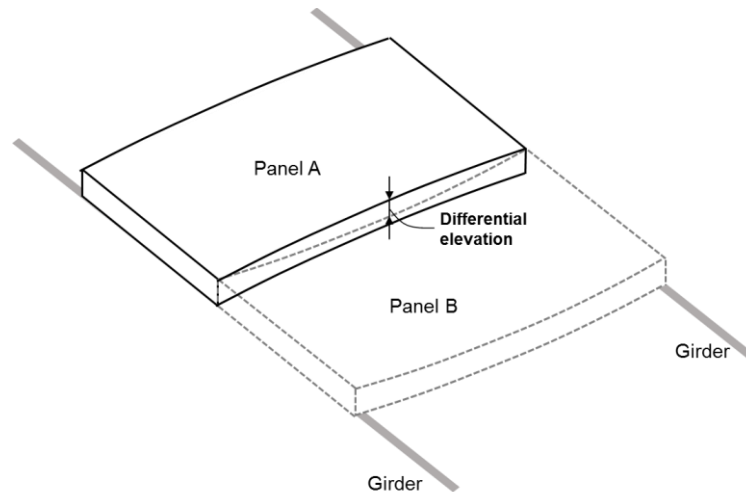
Fig. 5 Measurement of differential elevation between adjacent panels

The differential elevation between adjacent elements is affected by two factors, (1) the surface distortion of individual elements, and (2) the erection errors in the assemblage of elements. However, since the erection errors are unknown until completion of erection, in this study, only the surface distortion is considered when measuring the differential elevation. The tolerance value of the differential elevation varies for different types of precast concrete elements. For differential elevation between adjacent bridge deck panels, the tolerance value is ¾ inch (19 mm) (PCI 2000).

The measurement of differential elevation between adjacent elements is particularly important when adjacent elements have opposite distortions. Fig. 5 shows an example, where panel A has positive bowing while panel B has negative bowing. In this case, the two bowing features are additive when measuring the differential elevation between the two panels. Even though the bowing of two panels is within the tolerance, the resulting differential elevation may exceed the tolerance.

3. Proposed SFDI techniques

The proposed SFDI techniques using laser scanning technology consist of four steps, which are (1) acquisition of laser scanned data, (2) coordinate transformation, (3) estimation of surface flatness, and (4) estimation of surface distortion, as illustrated in Fig. 6. The details of the proposed techniques are described in the following subsections.

3.1 Acquisition of laser scanned data

Once the target surface to be inspected is determined, a laser scanner is used to acquire the laser scanned data of the target surface. As illustrated in Fig. 7, the direction from the laser scanner to the center of the target surface is perpendicular to the target surface. Such a scanning setting can minimize the incident angle of the laser beams with respect to the target surface, resulting in less

measurement noise. Here, the incident angle of laser beams denotes the angle between the laser beam direction and the normal vector of the target surface. After obtaining the laser scanned data, the portion of data which belong to the target surface are selected from the raw laser scanned data, in order to facilitate the subsequent data processing.

3.2 Coordinate transformation

Once the laser scanned data corresponding to the target surface are obtained, coordinate transformation is conducted. The raw laser scanned data (Fig. 8(a)) obtained from the laser scanner are presented in the scanner's coordinate system, which is related to the location and orientation of the scanner. In such a coordinate system, it is difficult to extract necessary information to conduct SFDI. Therefore, coordinate transformation which transforms the laser scanned data into a custom coordinate system is performed as follows. (1) Select three corner points of the target surface from the scanned data. Arbitrarily three corners out of four are determined and for each corner, a scanned data point is selected near this corner.
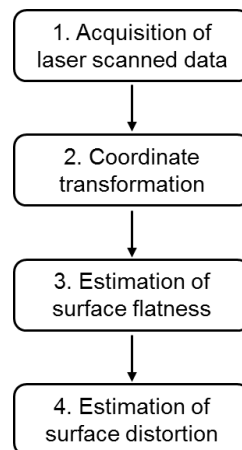

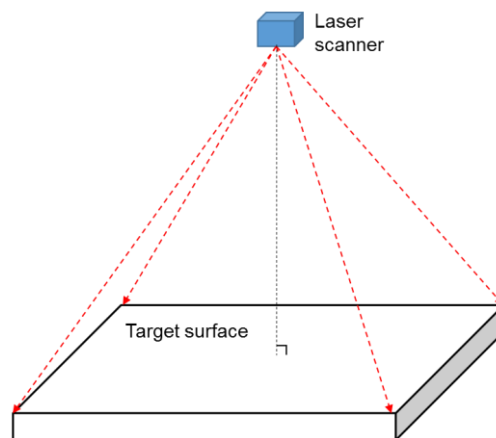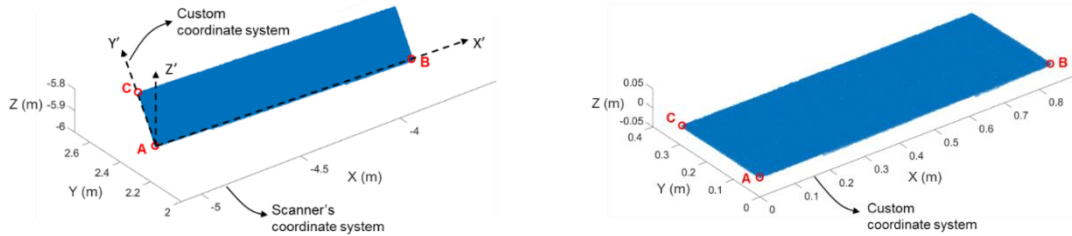Fig. 6 Overview of the proposed SFDI techniques

Fig. 7 Schematic of the scanning configuration

(a) Laser scanned data in the scanner's coordinate system

(b) Laser scanned data in the custom coordinate system after coordinate transformation

Fig. 8 Coordinate transformation of the laser scanned data

As shown in Fig. 8(a), points A, B and C are selected as corner points. (2) Create a custom coordinate system. The location of point B (or point C) is firstly slightly adjusted so that line AB is perpendicular to line AC. Then, the custom coordinate system is created by taking point A as the origin, the direction of AB as the X axis (X' in Fig. 8(a)) and the direction of AC as the Y axis (Y' in Fig. 8(a)). The Z axis (Z' in Fig. 8(a)) is automatically derived based on the directions of the X and Y axes because the Z axis is perpendicular to the XY plane. (3) Conduct coordinate transformation. The laser scanned data are transformed from the scanner's coordinate system into the newly created custom coordinate system by a rigid transformation. The scanned data after transformation are shown in Fig. 8(b).

3.3 Estimation of surface flatness

As the measurement of surface flatness, the F_F number is estimated from the laser scanned data as follows. (1) Place the sample measurement lines and sample reading points according to the requirements specified in ASTM (2008). (2) Obtain the elevations of the sample reading points. As shown in Fig. 9, empty dots represent the laser scanned data points on the target surface. For each sample reading point, its elevation is obtained from the elevation of its nearest laser scanned data point. (3) Calculate the F_F number of the surface based on the elevations of the sample reading points. Furthermore, to improve the reliability of the result, the F_F number is calculated iteratively for 1,000 times and take the average value. For each time, while keeping the number of the sample measurement lines and the relative locations between them unchanged, the distances from the sample measurement lines to the surface boundaries are different, determined by a random number. This random number follows a uniform distribution in the interval of [0 1].

3.4 Estimation of surface distortion

Warping, bowing and differential elevation between adjacent elements are all measured based on the elevations of the edges or corners of the surface. Therefore, edge points and corner points are extracted from the laser scanned data to represent the edges and corners of the surface.

As shown in Fig. 10, the laser scanned data, which are represented by dots, are arrayed in rows and columns. This is resulted from the horizontal and vertical rotation of the scanner head when the laser scanner is working. Hence, each laser scanned data point can be expressed by its location

of (row index, column index). Firstly, the first and last data points in each row and each column are extracted as edge points (filled dots) of the four edges of the surface. For example, the edge points of the top edge are extracted as the first data point in each column, i.e., points (1, 1), (1, 2)… (1, 12). Secondly, if a data point is an edge point of two different edges, it becomes a corner point (dark filled dots). For example, point (1, 1) is an edge point of both the top edge and the left edge. Then point (1, 1) becomes a corner point, which represents the left top corner of the surface. A total of four corner points are extracted, representing the four corners of the surface.

Once the edge points and corner points are extracted, three measurements of surface distortion are estimated. (1) Warping of each corner is estimated based on the elevations of the four corner points. For example, warping of the left top corner is measured as the deviation of corner point (1, 1) from the plane containing corner points (1, 12), (5, 1), and (5, 12). (2) Bowing of each edge is estimated based on the elevations of the edge points of this edge and is measured at the location of each edge point along the edge. For example, the two endpoints of the top edge are represented by corner point (1, 1) and corner point (1, 12), as shown in Fig. 11. Hence, its bowing is measured as the deviation of each edge point from the line containing the two endpoints, e.g., the measured bowing at the location of edge point (1, 7) shown in Fig. 11. Since the top edge has a total of 12 edge points, 12 bowing measurements are obtained along the top edge. (3) Differential elevation between adjacent elements is estimated based on the elevations of the edge points of the edge which is connected to the adjacent element. Similar to bowing, the differential elevation is measured at the location of each edge point along the edge, yielding a series of differential elevation measurements.
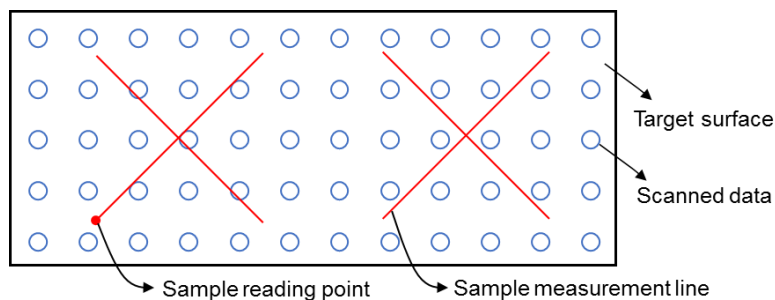

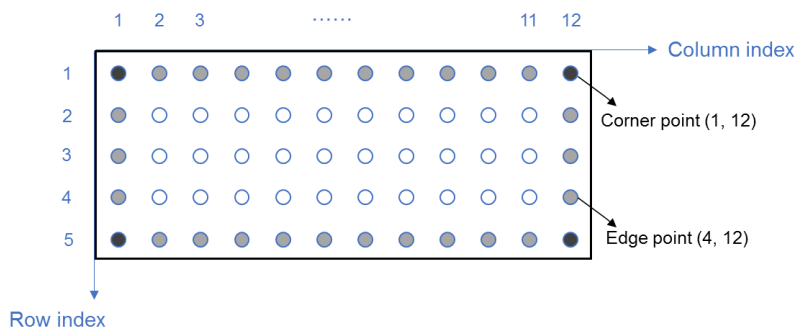Fig. 9 Estimation of the FF number from the laser scanned data

Fig. 10 Extraction of the edge points and corner points from the laser scanned data for surface distortion estimation
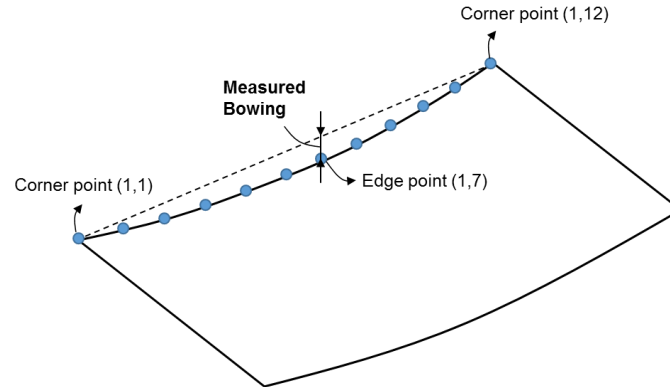
Fig. 11 Measurement of bowing of the top edge from the laser scanned data

4. Validation experiments

To validate the proposed SFDI techniques, scanning experiments were conducted on test specimens and the proposed techniques were applied to the laser scanned data of the test specimens. The measured surface flatness and distortion from the laser scanned data were compared to the actual ones, which were obtained from the designed surface geometries of the test specimens, to evaluate the accuracy of the proposed techniques.

4.1 Test specimens and experimental set-up

A total of four test specimens were manufactured and used for the validation experiments, as shown in Fig. 12. In order to artificially generate surface flatness and distortion of the specimens, a MakerBot (2015) Replicator Desktop 3D printer was used to manufacture the specimens. The 3D printer provided a layer resolution of 0.1 mm and had a circular nozzle diameter of 0.4 mm. The XY and Z positioning precision was 0.01 mm and 0.0025 mm, respectively. Considering the accurate geometries provided by the 3D printer, the actual surface flatness and distortion of the specimens could be obtained from the designed surface geometries of the specimens. However, the 3D printer also had a limitation in that it could only manufacture objects within the size of 285 mm (length) × 153 mm (width) × 155 mm (height), which limited the size of specimens. In the validation experiments, the four specimens were thus sized at 200 mm (length) × 100 mm (width) × 5-10 mm (height).

Specimen I and specimen II were designed for surface flatness inspection. The surface of each specimen was divided into square cells by grids along the horizontal and vertical directions, with a grid size of 5 mm. Furthermore, each square cell was subdivided into two triangles by a diagonal. For each grid point, which was also a vertex of the triangles, a Gaussian random number was generated to determine its elevation. Then, each triangle became a small planar surface which was determined by the elevations of its three vertices. Finally, all the triangles made up the whole surface of each specimen. In this study, two Gaussian random numbers with the same mean value of 6 mm, but different standard deviations of 1 mm and 2 mm, were applied to specimen I and specimen II, respectively. Therefore, specimen I had a flatter surface than specimen II.
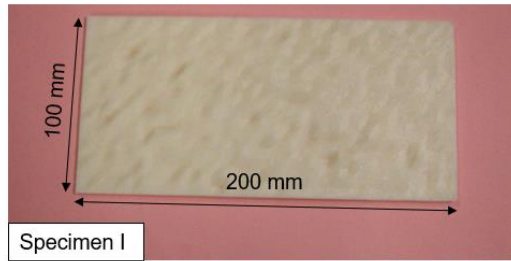
(a) Specimen I with non-flat surface
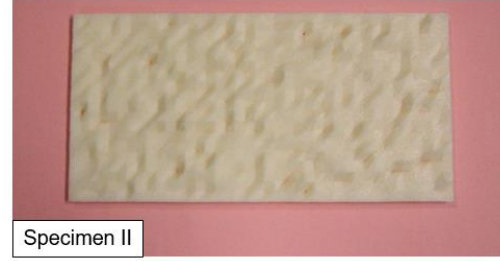
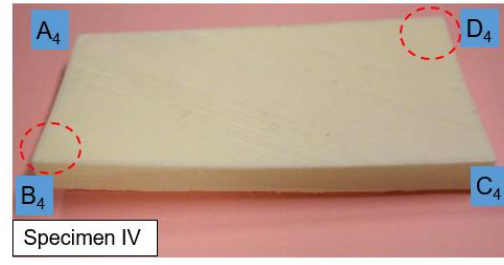(b) Specimen II with non-flat surface (less flat than specimen I)

(c) Specimen III with upward distortion at corner D_3

(d) Specimen IV with upward distortions at corner B_4 and corner D_4

Fig. 12 Test specimens for the validation experiments

Specimen III and specimen IV were designed for surface distortion inspection, hence their surfaces had certain distortions, making the surfaces deviate from the true planes. As shown in Fig. 12(c), specimen III was designed with an upward distortion at corner D_3. The portion of the surface composed by corners A_3, C_3, and D_3 was higher than the true plane while the other portion was still on the true plane. The deviation of corner D_3 from the true plane was 15 mm, which was the maximum deviation throughout the surface. As shown in Fig. 12(d), specimen IV was designed with two upward distortions at corner B_4 and corner D_4. The whole surface was higher than the true plane and only the line A_4C_4 had the same elevation as the true plane. The deviations of corner B_4 and corner D_4 from the true plane were 12 mm and 8 mm, respectively.

Fig. 13 shows the experimental set-up of the validation experiments. The laser scanned data of the test specimens were acquired by a FARO Focus 3D laser scanner, which provided range measurement accuracy of ±2 mm at a scanning distance of 20 m (FARO 2015). The scanning distance from the laser scanner to the specimen was 1.2 m and the scanning angular resolution was 0.018°, providing a spatial resolution, i.e. the distance between two adjacent laser scanned data points, of 0.4 mm.

4.2 Data processing results

The laser scanned data of the specimens were processed by the proposed techniques through the four steps described in Section 3. Firstly, as shown in Fig. 14(a), the raw laser scanned data of the specimens were acquired by the laser scanner. Then, coordinate transformation was performed to transform the raw data from the scanner's coordinate system into a custom coordinate system,

as shown in Fig. 14(b). The next is to estimate the F_F number from the laser scanned data to evaluate the surface flatness of specimen I and specimen II. The quantities and locations of the sample measurement lines and the sample reading points distributed on the specimen surfaces are shown in Fig. 14(c). Since the specimens had a much smaller size than actual floor surfaces, the distances between two parallel sample measurement lines and between two sample reading points were adjusted to 40 mm and 10 mm, respectively. Finally, the warping, bowing and differential elevation between adjacent elements were estimated to evaluate the surface distortion of specimen III and specimen IV. Fig. 14(d) shows the edge points and corner points extracted from the laser scanned data, which were used to estimate the three measurements of surface distortion.

4.3 Accuracy analysis

To examine the accuracy of the proposed techniques, the measured surface flatness and distortion from the laser scanned data were compared to the actual surface flatness and distortion, which were obtained from the designed surface geometries of the 3D printed specimens.

4.3.1 Surface flatness

Table 2 shows the actual and measured F_F numbers of specimen I and specimen II, with discrepancies of 1.46 and 0.64 for the two specimens respectively. According to the surface flatness classification in Table 1, the difference between the F_F numbers of the two classes is 5, 10 or 20, which is much larger than the discrepancies (1.46 and 0.64). It can be inferred from the results that the measured F_F numbers can accurately evaluate surface flatness.
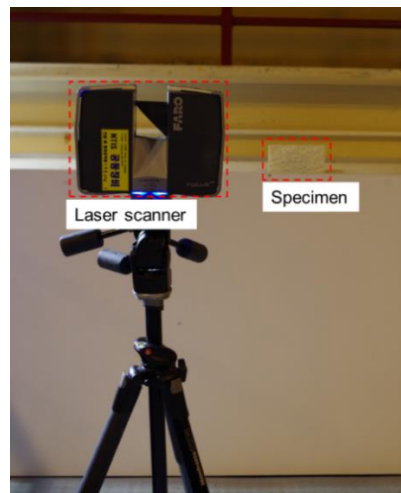

Fig. 13 Experimental set-up of the validation experiments

Table 2 The actual and measured FF number of specimen I and specimen II

	Actual F_F number	Measured F_F number	Discrepancy
Specimen I	20.44	21.90	1.46
Specimen II	9.16	9.80	0.64

(a) Acquisition of laser scanned data   (b) Coordinate transformation

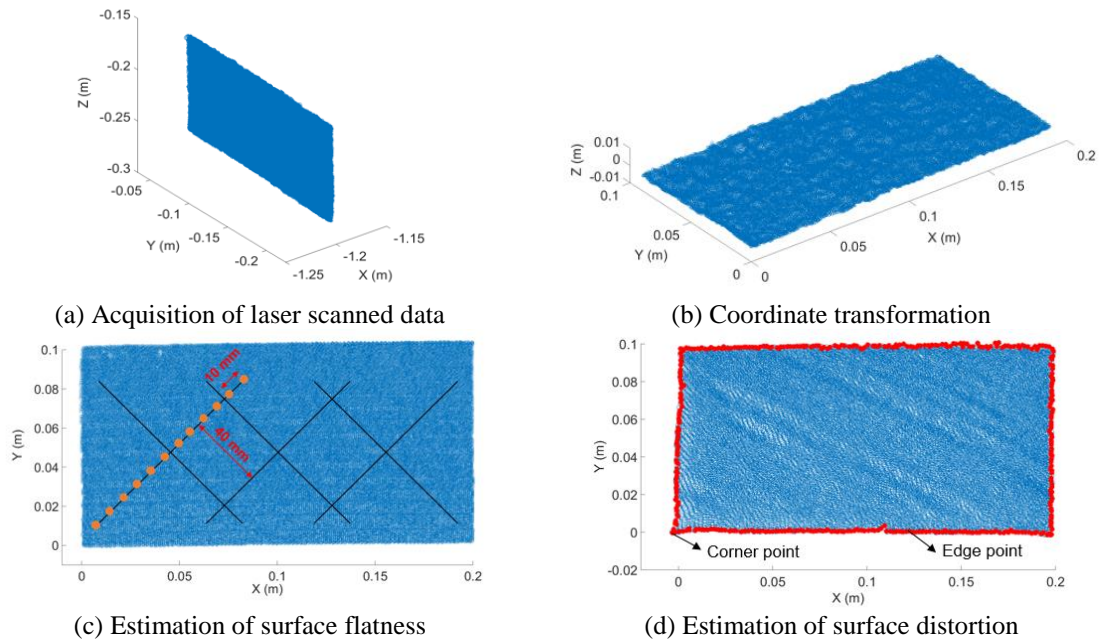(c) Estimation of surface flatness   (d) Estimation of surface distortion

Fig. 14 SFDI procedures of the test specimens

It is also shown that the measured F_F numbers of the two specimens are both larger than the actual F_F numbers, indicating that the measured surfaces are flatter than the actual surfaces. A possible reason is the "mean filter effect" of laser scanners. In fact, laser beams emitted from the laser scanner are circular and have a diameter of 3.8 mm at exit (FARO 2015) For this reason, a laser beam will fall on a circular or elliptical (depending on the incident angle of the laser beam) area of the specimen surface, with an area of more than 11 mm^2. Since the surface elevations can vary within the area, the resulting measurement will be the averaged elevation of the area, acting like a mean filter. As a result, the peak and valley values of the surface elevations will be reduced because of the "mean filter effect" and the surface appears flatter in the laser scanned data.

4.3.2 Surface distortion

Table 3 shows the actual and measured warping of specimen III and specimen IV. Since warping is measured at all the four corners of a surface, only the maximum warping among the four corners is shown in the figure. The discrepancies between the actual and measured warping are 1.5 mm and 1.2 mm for the two specimens, respectively. In comparison with the tolerance for warping (5 mm for a 1 m wide surface), the measured warping is sufficiently accurate to evaluate surface warping. Note that 1 m wide surface is taken as an example to calculate the tolerances since actual precast concrete elements usually have sizes larger than 1 m.

Figs. 15 and 16 show the actual and measured bowing of specimen III and specimen IV along all the four edges. For each edge, the magnitudes of bowing at different locations are represented by the lengths of the line segments which are perpendicular to the edge. Take edge A_3D_3 in Fig. 15(a) as an example, a series of vertical line segments are drawn above edge A_3D_3 and a curve connects the top endpoints of all these line segments. The length of vertical line segments is

proportional to the magnitudes of bowing. Line segments drawn outside the surface indicate negative bowing; and vice versa. Therefore, the longest vertical line segment indicates the maximum bowing (-4.1 mm) along edge A_3D_3.

For each edge of specimen III, the average discrepancy between the actual and measured bowing is calculated, which is 0.4 mm (top edge), 0.2 mm (bottom edge), 0.4 mm (left edge), and 0.4 mm (right edge), respectively. Similarly, for specimen IV, the discrepancy is 0.3 mm (top edge), 0.2 mm (bottom edge), 0.3 mm (left edge), and 0.3 mm (right edge), respectively. In comparison with the tolerance for bowing (2.8 mm for a 1 m long edge), the proposed measurement method of bowing provides results with sufficient accuracy to evaluate surface bowing.

Table 3 The actual and measured warping of specimen III and specimen IV

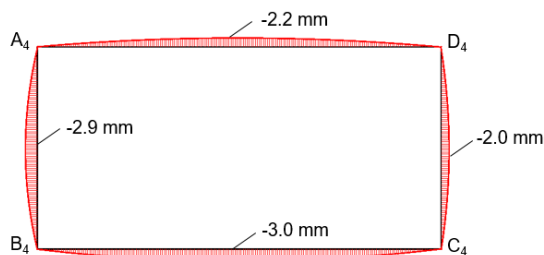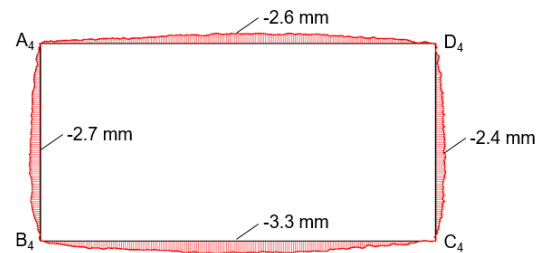|	Actual warping (mm)	Measured warping (mm)	Discrepancy (mm)
Specimen III	15.0	16.5	1.5
Specimen IV	18.4	19.6	1.2
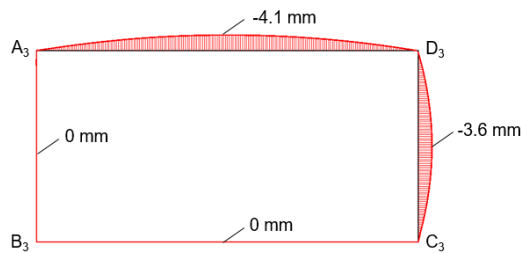
(a) The actual bowing of specimen III
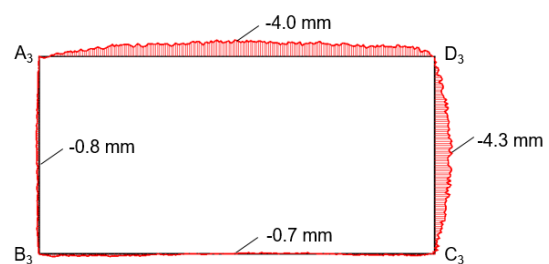
(b) The measured bowing of specimen III from the laser scanned data

Fig. 15 The actual and measured bowing of specimen III

(a) The actual bowing of specimen IV

(b) The measured bowing of specimen IV from the laser scanned data

Fig. 16 The actual and measured bowing of specimen IV

(a) The actual differential elevation

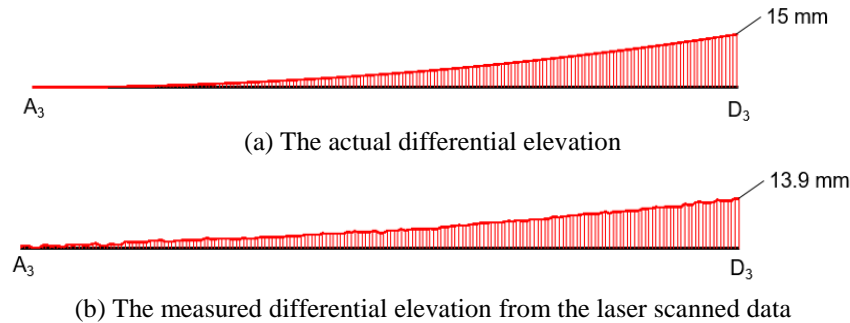(b) The measured differential elevation from the laser scanned data

Fig. 17 The actual and measured differential elevation between specimen III and its adjacent element along edge A_3D_3

Fig. 17 shows the actual and measured differential elevation between specimen III and its adjacent element along edge A_3D_3. Assumptions are made that (1) corners A_3, B_3 and C_3 of specimen III are placed on the supporting plane, (2) edge A_3D_3 of specimen III is connected to its adjacent element, and (3) the adjacent element is well manufactured. Similar to bowing, the magnitudes of differential elevations are represented by the lengths of the vertical line segments along edge A_3D_3. The maximum values of the actual and measured differential elevations are 15.0 mm and 13.9 mm respectively, showing a discrepancy of 1.1 mm. The average discrepancy between the actual and measured differential elevations is 0.8 mm. In comparison with the tolerance (19 mm), the proposed measurement technique provides accurate results to evaluate the differential elevation between adjacent elements.

5. Application of the proposed techniques to bridge deck panels

To further examine the applicability of the proposed techniques on actual precast concrete elements, scanning experiments were conducted on two precast concrete bridge deck panels, denoted as panel I and panel II, and the laser scanned data of the panels were processed by the proposed techniques.

5.1 The bridge deck panels and experimental set-up

The two precast concrete bridge deck panels were manufactured in the same precast concrete plant with the same designed dimensions of 12,600 mm × 2,480 mm, as shown in Fig. 18(a). Each panel has a total of 25 shear pockets with identical sizes of 440 mm × 140 mm, which are designed to connect the panel to the girders. Fig. 18(b) shows the experimental set-up of the scanning experiment for panel I and it is similar for panel II. Panel I is marked with dashed red lines and its four corners are denoted as A_5, B_5, C_5, and D_5. Similarly, for panel II, its four corners are denoted as A_6, B_6, C_6, and D_6. The laser scanner was placed on the crane and the scanning distance from the scanner to the panel was 8 m. In this experiment, the scanning angular resolution was set as 0.018° so that the scanning time was less than 10 minutes. The laser scanner had a measurement range of 120 m and measurement error of ± 2 mm.

(a) Dimensions of the bridge deck panels

(b) The experimental set-up of the scanning experiment for panel I
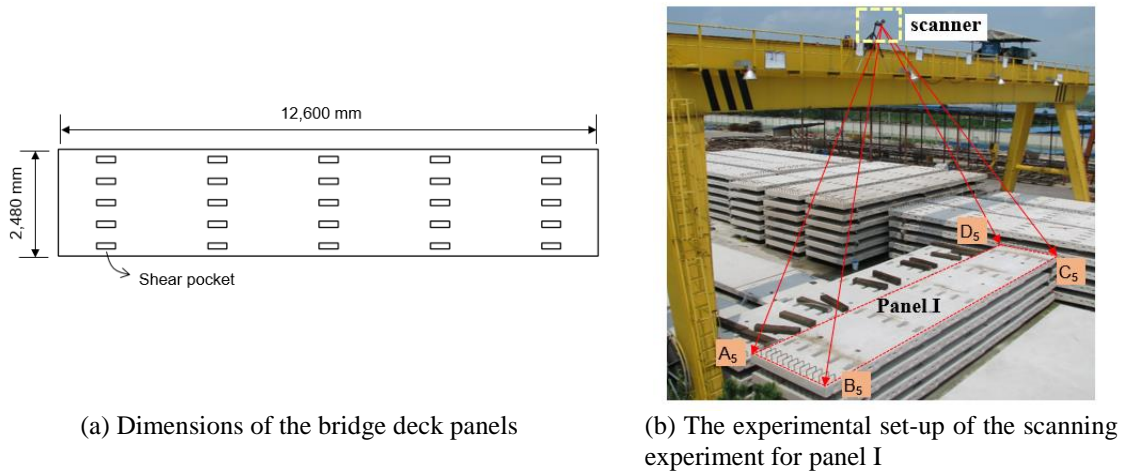
Fig. 18 Dimensions of the bridge deck panels and the scanning experiment

5.2 Data processing results

The proposed techniques were applied to the laser scanned data of the panels, as illustrated in Fig. 19. The same laser scanner as used in the validation experiments described in Section 4 was used to acquire the laser scanned data of the panels, as shown in Fig. 19(a). Then, a custom coordinate system was created and the laser scanned data were transformed into the new coordinate system, as shown in Fig. 19(b). After the coordinate transformation, one corner of the panel was located at the origin and two edges of the panel overlapped with the X and Y axes respectively. To evaluate the surface flatness by the F_F number, a total of eight sample measurement lines were placed on the surface, as shown in Fig. 19(c). The orientations of all the lines were 45° to the longest boundary of the surface and each line had an identical length of 3.3 m, with 12 sample reading points distributed along it. To eliminate the influence of the shear pockets, sample measurement lines are carefully placed to avoid any overlapping with the shear pockets. Finally, to evaluate the surface distortion, the edge points and corner points were extracted from the laser scanned data, as shown in Fig. 19(d), in order to estimate the three measurements of surface distortion.

5.3 Analysis of inspection results

5.3.1 Surface flatness

The estimated F_F numbers of panel I and panel II are 16.5 and 24.0, respectively. According to the surface flatness classification shown in Table 1, panel I belongs to the bullfloated class and panel II belongs to the straightedged class, indicating that panel I is not as flat as panel II.

5.3.2 Surface distortion

Table 4 shows the measured warping at the four corners of panel I and panel II, with the maximum warping of -5.4 mm and -4.8 mm, respectively. Since the tolerance for warping is 12.4

mm (calculated as 1.5 mm per 300 mm of the distance to its nearest adjacent corner) for the panels, the warping of both panels does not exceed the tolerance. Regarding the magnitudes of warping, panel I and panel II do not present much difference, although panel I has larger warping in average.

Fig. 20 shows the bowing of panel I and panel II along the four edges, and the maximum bowing along each edge is shown in the figure. The tolerance for bowing is 6.9 mm (calculated as length/360, to a maximum of 1 inch (25 mm)) for the short edges and 25 mm (calculated as length/360, to a maximum of 1 inch (25 mm)) for the long edges. The results show that, for panel I, the bowing of edges A_5B_5, B_5C_5 and D_5A_5 exceeds the corresponding tolerances; for panel II, the bowing of all the four edges is within the tolerances. It can be concluded that panel I has larger bowing than panel II.

Fig. 21 shows the differential elevation between panel I and panel II. It is assumed that (1) corners A_5, B_5 and C_5 of panel I are located on the supporting plane, (2) corners A_6, C_6 and D_6 of panel II are located on the supporting plane, and (3) edge B_5C_5 of panel I is connected with edge A_6D_6 of panel II. According to the measurement result in Fig. 21, the maximum differential elevation along edge B_5C_5 (A_6D_6) is 26.2 mm, which exceeds the tolerance of 19 mm. It indicates that panel I and panel II cannot be connected to each other; however, it is still possible to connect them to other panels as long as the differential elevation between adjacent panels does not exceed the tolerance. Furthermore, if a series of identical panels are connected next to each other on the same supporting plane, it will be an interesting topic that how to decide the sequences of the panels so that the total differential elevations between adjacent panels are minimized.
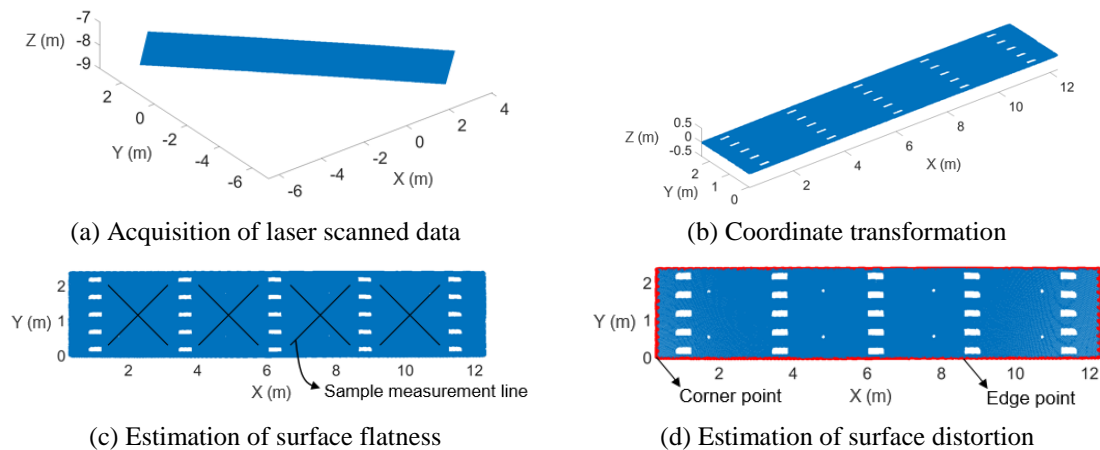

(a) Acquisition of laser scanned data

(b) Coordinate transformation

(c) Estimation of surface flatness

(d) Estimation of surface distortion

Fig. 19 SFDI procedures of the bridge deck panels

Table 4 The measured warping at the four corners of panel I and panel II

	Corner A_5/ A_6 (mm)	Corner B_5/ B_6 (mm)	Corner C_5/ C_6 (mm)	Corner D_5/D_6 (mm)	Maximum (mm)
Panel I	-5.1	+5.0	-5.4	+4.6	-5.4
Panel II	+3.6	-4.8	+4.2	-3.8	-4.8

(a) The bowing of panel I
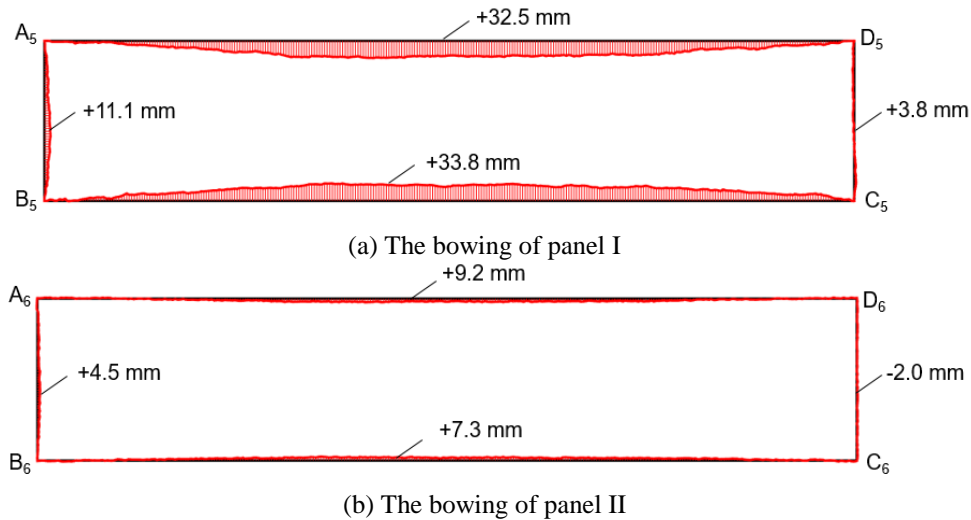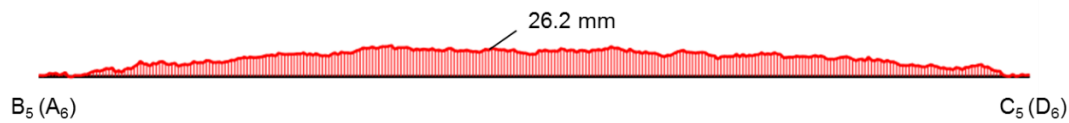

(b) The bowing of panel II

Fig. 20 The bowing of panel I and panel II along the four edges

Fig. 21 The differential elevation between panel I and panel II along edge B_5C_5 (A_6D_6)

It is observed from the above inspection results that panel I has substantially less flat surface compared to panel II, showing a difference of 7.5 between the two F_F numbers. Considering that the two panels are manufactured in the same precast concrete plant with the same techniques, the casting process will not result in such an obvious flatness difference. Instead, one possible reason for the flatness difference is that surface flatness measured by the F_F number is correlated with the surface distortion. For example, Figs. 22(a) and 22(b) show a surface before and after a distortion occurs, respectively. The surface is originally in a plane but presents an out-of-plane curvature due to a distortion. In this case, the F_F number of the surface will surely become smaller after the distortion occurs. Similarly, since panel I has larger surface distortion compared to panel II, the F_F number of panel I is affected more heavily by the surface distortion, resulting in a smaller F_F number. Due to the correlation explained above, when looking at the F_F number of a surface, the effect of surface distortion needs to be considered at the same time. For precast concrete elements, some surface distortion is resulted from improper storage environments in precast concrete plants and the distortion can be eliminated or reduced after the elements are erected on construction sites. In this case, the F_F number measured in plants cannot be directly used for quality inspection. Instead, it is necessary to cancel the effect of surface distortion when measuring the F_F number so that the measured F_F number can reflect the actual surface flatness after the element is erected.

Normal surface

Distorted surface

(a) Cross section view of a normal surface without distortion

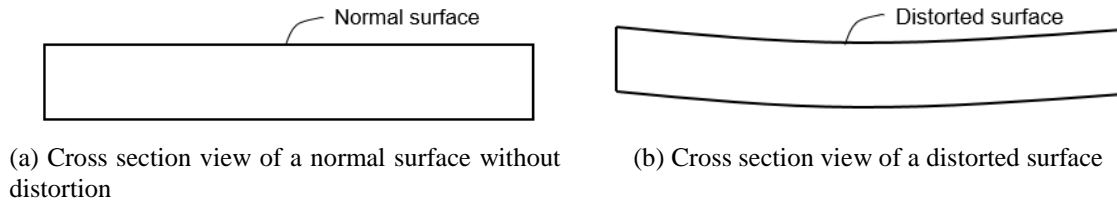(b) Cross section view of a distorted surface

Fig. 22 A surface before and after a distortion occurs

6. Conclusions

To provide solutions that can conduct surface inspection more efficiently and accurately, this study proposes SFDI techniques for precast concrete elements using laser scanning technology. Firstly, the laser scanned data of the target surface are obtained by a 3D laser scanner. Then, the laser scanned data are transformed from the scanner's coordinate system to a custom coordinate system to facilitate further processing. Thirdly, the F_F number is estimated from the laser scanned data to evaluate the surface flatness. Lastly, three different measurements, warping, bowing, and differential elevation between adjacent elements, are estimated to evaluate the surface distortion in different aspects.

To validate the proposed techniques, validation experiments were conducted on four small scale test specimens, which were manufactured by a 3D printer. The proposed techniques were applied to the laser scanned data of the specimens and the measured surface flatness and distortion were compared to the actual values, which were obtained from the designed surface geometries of the specimens. The experimental results show that the measured F_F number is sufficiently accurate (error less than 1.5) to evaluate the surface flatness; and for surface distortion, the measured warping, bowing and differential elevation between adjacent elements all have enough accuracy (error less than 2 mm) to evaluate the surface distortion. Furthermore, scanning experiments were conducted on two actual precast concrete bridge deck panels. The experiment results show that the proposed techniques can be successfully applied to actual precast concrete elements as well. According to the manual of the laser scanner, to obtain accurate measurement, the ambient temperature should be between 5℃ - 40℃ and the humidity condition should be non-condensing. These two requirements were fulfilled in the experiments.

Regarding surface flatness inspection, this study has validated the F_F number results from the laser scanned data by using 3D printed test specimens. Regarding surface distortion inspection, this study has developed and validated techniques that estimate warping, bowing and differential elevation between adjacent elements from the laser scanned data. The three measurements evaluate surface distortion from the perspective of not only individual precast concrete elements but also complete precast concrete systems. In addition, this study has preliminarily discussed the correlation between the F_F number and the surface distortion, which can be further studied in future work.

Although the results of this study are satisfactory, there are some limitations or remaining problems, which can be potential future work. (1) Currently, this study is limited to precast concrete elements with rectangular surfaces. The inspection techniques for non-rectangular elements remain to be developed. (2) As stated in Section 5.3, with a series of identical precast concrete panels, it is an interesting topic to figure out how to decide the sequences of the panels so

that the total differential elevations are minimized. (3) The correlation between the F_F number and the surface distortion is discussed in Section 5.3. However, the approach to cancelling the effect of surface distortion when measuring the F_F number remains to be developed.

Acknowledgements

References

Alhassan, M. (2011), *State-of-the-Art Report on Full-Depth Precast Concrete Bridge Deck Panels*.

Amann, M.C., Bosch, T., Lescure, M., Myllyla, R. and Rioux, M. (2001), "Laser ranging: a critical review of usual techniques for distance measurement", *Opt. Eng.*, **40**(1), 10-19.

American Concrete Institute (ACI) (2006), *ACI 117-06—Specifications for Tolerances for Concrete Construction and Materials and Commentary*.

ASTM (2008), *ASTM E 1155-96 —Standard Test Method for Determining FF Floor Flatness and FL Floor Levelness Numbers*.

Bai, H., Ye, X.W., Yi, T.H., Dong, C.Z. and Liu, T. (2015), "Multi-point displacement monitoring of bridges using a vision-based approach", *Wind Struct.*, **20**(2), 315-326.

Ballast, D.K. (2007), *Handbook of Construction Tolerances*. John Wiley & Sons.

Bosché, F. (2010), "Automated recognition of 3D CAD model objects in laser scans and calculation of as-built dimensions for dimensional compliance control in construction", *Adv. Eng. Inform.*, **24**(1), 107-118.

Bosché, F. and Biotteau, B. (2015), "Terrestrial laser scanning and continuous wavelet transform for controlling surface flatness in construction–A first investigation", *Adv. Eng. Inform.*, **29**(3), 591-601.

Bosché, F. and Guenet, E. (2014), "Automating surface flatness control using terrestrial laser scanning and building information models", *Automat. Constr.*, **44**, 212-226.

Bosché, F., Ahmed, M., Turkan, Y., Haas, C.T. and Haas, R. (2015), "The value of integrating Scan-to-BIM and Scan-vs-BIM techniques for construction monitoring using laser scanning and BIM: The case of cylindrical MEP components", *Automat. Constr.*, **49**, 201-213.

British Standard Institution (BSI) (2009), *BS 8204—Screeds, Bases and In Situ Flooring*.

El-Omari, S. and Moselhi, O. (2008), "Integrating 3D laser scanning and photogrammetry for progress measurement of construction work", *Automat. Constr.*, **18**(1), 1-9.

FARO (2015), *FARO Focus 3D laser scanner*. http://www.faro.com/.

Glass, J. (2000), *The Future for Precast Concrete in Low-rise Housing*. Leicester: British Precast Concrete Federation.

Kim, M.K., Sohn, H. and Chang, C.C. (2014), "Automated dimensional quality assessment of precast concrete panels using terrestrial laser scanning", *Automat. Constr.*, **45**, 163-177.

Makerbot (2015), *Makerbot replicator 3D printer*. https://www.makerbot.com/.

Monserrat, O. and Crosetto, M. (2008), "Deformation measurement using terrestrial laser scanning data and least squares 3D surface matching", *ISPRS J. Photogramm.*, **63**(1), 142-154.

Park, H.S., Lee, H.M., Adeli, H. and Lee, I. (2007), "A new approach for health monitoring of structures: terrestrial laser scanning", *Comput-Aided Civ. Inf.*, **22**(1), 19-30.

Phares, B.M., Washer, G.A., Rolander, D.D., Graybeal, B.A. and Moore, M. (2004), "Routine highway bridge inspection condition documentation accuracy and reliability", *J. Bridge Eng.*, **9**(4), 403-413.

Precast/Prestressed Concrete Institute (PCI) (2000), *135-Tolerance Manual for Precast and Prestressed Concrete Construction.*

Tang, P., Huber, D. and Akinci, B. (2010), "Characterization of laser scanners and algorithms for detecting flatness defects on concrete surfaces", *J. Comput. Civil Eng.*, **25**(1), 31-42.

Teza, G., Galgaro, A. and Moro, F. (2009), "Contactless recognition of concrete surface damage from laser scanning and curvature computation", *NDT&E Int.*, **42**(4), 240-249.

Turkan, Y., Bosche, F., Haas, C.T. and Haas, R. (2012), "Automated progress tracking using 4D schedule and 3D sensing technologies", *Automat. Constr.*, **22**, 414-421.

Wacker, J.M., Eberhard, M.O. and Stanton, J.F. (2005), *State-of-the-art Report on Precast Concrete Systems for Rapid Construction of Bridges* (No. WA-RD 594.1). Washington State Department of Transportation.

Xiong, X., Adan, A., Akinci, B. and Huber, D. (2013), "Automatic creation of semantically rich 3D building models from laser scanner data", *Automat. Constr.*, **31**, 325-337.

Yee, A.A. and Eng, P.H.D. (2001), "Social and environmental benefits of precast concrete technology", *PCI J.*, **46**(3), 14-19.

Yeum, C.M. and Dyke, S.J. (2015), "Vision-based automated crack detection for bridge inspection", *Comput-Aided Civ. Inf.*

Yi, T.H., Li, H.N. and Gu, M. (2013), "Experimental assessment of high-rate GPS receivers for deformation monitoring of bridge", *Measurement*, **46**(1), 420-432.

Yi, T.H., Li, H.N. and Gu, M. (2013), "Wavelet based multi-step filtering method for bridge health monitoring using GPS and accelerometer", *Smart Struct. Syst.*, **11**(4), 331-348.